Information propagated by longitudinal pulses near a van der Waals phase transition

Matan Mussel*

Department of Physics and Center for Biophysics and Quantitative Biology, University of Haifa, Haifa 3103301, Israel

(Received 14 February 2023; accepted 30 August 2023; published 19 September 2023)

Longitudinal pulses that propagate in a medium near a van der Waals phase transition have a sigmoidal dependence on the strength of the stimulus arising from the phase structure. This response resembles the all-or-nothing property of action potentials, which raises the question if an acoustic system near a phase transition can be suitable for material-based neuromorphic computation. Herein, we investigate how information about the stimulus is stored within these pulses. We find that (1) the pulse propagates in parallel both digital and analog information about the stimulus amplitude; (2) the pulse encodes the type of stimulus, for instance, mechanical or thermal; and (3) a collision between two pulses stores information about both stimuli and may be used as a fading memory. Our results unravel a rich encoding of information in a phenomenon that is both common in a plethora of materials and mimics neuronal signaling. In addition, we show that these pulses carry more information than is typically considered by models of neural computation. Therefore, this phenomenon is an excellent candidate for *in materio* computation.

DOI: 10.1103/PhysRevE.108.034209

I. INTRODUCTION

Longitudinal waves propagate through a medium by means of local compression and rarefaction, where mechanical forces are exerted on adjacent regions and transfer elastic and kinetic energy. This is a universal phenomenon, emerging from the conservation of momentum in practically any material [1]. In the small amplitude limit, the conservation and constitutive equations simplify into the linear wave equation, which indeed captures many properties of longitudinal waves in water and air. For example, small amplitude longitudinal waves are produced at a broad range of amplitudes and frequencies, their local changes in density and pressure are linearly proportional to one another, and the waves pass through each other without being disturbed. Other phenomena, such as shock waves, solitons, and rogue waves, are not described by the linear wave equation and require a more detailed description of the medium [2].

In this paper, we investigate the characteristics of nonlinear longitudinal waves that cause a reversible phase transition in the medium. The simplest hydrodynamic description includes the van der Waals (vdW) equation of state that accounts for the volume occupied by the particles of the medium and their short-range interparticle attraction forces. These characteristics are sufficient to generate a steep transition in density. A vdW-like phase diagram is common in a plethora of soft materials, including the liquid-vapor transition in fluids composed of a single species such as water and nitrogen [3], order-disorder transition in lipid membranes [4], volume transition in polymer gels [5], and metamaterial with microstructure instabilities [6]. Therefore, the study of longitudinal waves near a phase transition is relevant for many different systems.

Longitudinal pulses that reversibly cross a vdW-like phase transition share many similar properties with *action potentials*, electric signals that propagate along the lipid membrane of excitable living cells [7]. Both types of pulses have a sigmoidal response to stimulation strength, they annihilate upon collision, and the two phenomena have a resembling characteristic shape [8–11]. In addition, the structure of the governing hydrodynamic equations is analogous to the generalized FitzHugh-Nagumo model [12]. Although the pulse duration and propagation velocity differ between materials, an additional resemblance to action potentials exists in lipid interfaces near the order-disorder transition, where both the time and velocity scales are the same as those of action potentials, respectively, $\sim 10^{-3}$ to 1 s and $\sim 10^{-1}$ to 10^{2} m/s [9,13]. Moreover, in charged lipid membranes, an associated variation in electric potential copropagates with the longitudinal pulse with a scale of $\sim$1–100 mV, like action potentials [13–15].

Intense research on action potentials led to the successful development of biologically inspired computing schemes, such as artificial neural network models, capable of solving complex tasks that benefit from adaptivity and learning from examples [16,17]. Therefore, the close resemblance between action potentials and longitudinal pulses near a phase transition suggests that the latter might be harnessed for computing schemes inspired by neuronal signaling. Exploiting the properties of a medium to perform neural algorithms offers many potential advantages over classical von Neumann computing, such as parallelism, reduced energy consumption, and enhanced computational performance [18–20].

Indeed, unconventional wave-based computation has previously been explored in waves that either superimpose or annihilate upon collision, offering computational algorithms at different levels of sophistication [21–29]. However, in those works, the propagating waves are described using a single

*mmussel@univ.haifa.ac.il

variable. For small amplitude longitudinal waves, these computational schemes can be sufficient because the oscillatory variations of the density and pressure are linearly proportional to one another. However, at the nonlinear limit, the variations of these observables are no longer proportional, and the information about the stimulus is cast into a high-dimensional space of observables [13]. This property makes an acoustic system extremely suitable for material-based neuromorphic computing [22].

An important step in the attempt to harness longitudinal waves to perform neuroinspired computation, which is the goal of this paper, is to understand how information about the stimulus is stored in the pulse. Here, we demonstrate that, compared with standard neural models, more information about the stimulus is stored in longitudinal pulses: (1) The multidimensionality of the pulse contains more than an all-or-nothing and includes both digital and analog information about the stimulus amplitude. (2) The pulse contains information about the type of stimulus, for instance, if it was stimulated mechanically or by locally increasing the temperature. (3) Collision sites are longlasting (∼5 times the pulse duration) and may be used as locations for short-term memory. Our results emphasize the richness of the phenomenon; consequently, such a system is an excellent candidate for material-based computing that mimics and potentially even surpasses neural network dynamics.

II. MODEL DESCRIPTION

To explore the information stored in longitudinal pulses that reversibly cross a phase transition, we investigate a hydrodynamic model that includes the simplest form of phase transition: the vdW fluid model [11,12,30]. The compressible fluid model couples five variables of the system: specific volume, pressure, temperature, energy, and velocity fields, respectively, $w,\ p,\ \theta, E$, and v, using three conservation laws and two constitutive relations. The fluid density is inversely proportional to the specific volume $\rho = w^{-1}$. For simplicity, we vary only one spatial dimension of the medium and study plane-wave solutions. In the Lagrangian frame of reference and in dimensionless units designated using the tilde notation, the conservation of mass, momentum, and energy, are, respectively [11,12],

$$\begin{aligned}\partial_{\tilde{t}}\tilde{w} &= \partial_{\tilde{X}}\tilde{v},\\ \partial_{\tilde{t}}\tilde{v} &= \partial_{\tilde{X}}\tilde{\tau},\\ \partial_{\tilde{t}}\tilde{E} &= \partial_{\tilde{X}}(\tilde{\tau}\tilde{v}) + \partial_{\tilde{X}}(\tilde{C}\partial_{\tilde{X}}\tilde{v}\partial_{\tilde{X}}\tilde{w}) + \tilde{k}\partial_{\tilde{X}}^2\tilde{\theta}.\end{aligned} \tag{1}$$

Here, $\tilde{\tau}$ is the dimensionless stress in the fluid:

$$\tilde{\tau} = -\tilde{p} + \partial_X\tilde{v} - \tilde{C}\partial_X^2\tilde{w}, \tag{2}$$

and $\tilde{X}$ is the dimensionless spatial coordinate in the Lagrangian frame of reference. The spatial coordinate $\tilde{X}$ (in the Lagrange frame) is related to the x axis (in the Euler frame) by the cumulative mass of fluid particles [31]:

$$\tilde{x} = \int \tilde{w}d\tilde{X}. \tag{3}$$

The proper time and length scales used to determine the dimensionless equations are

$$T = \frac{\zeta}{p_c}, \quad L = \zeta\sqrt{\frac{w_c}{p_c}}, \tag{4}$$

with ζ the dilatational viscosity, and $(w_c,\ p_c,\ \theta_c)$ are the critical specific volume, critical pressure, and critical temperature of the phase transition, respectively. More details about the dimensionless parameters, variables, and equations are provided in the supplemental material of Ref. [11].

The two vdW constitutive relations are

$$\begin{aligned}\tilde{p} &= \frac{8\tilde{\theta}}{3\tilde{w}-1} - \frac{3}{\tilde{w}^2},\\ \tilde{E} &= \frac{\tilde{v}^2}{2} + \tilde{c}_v\tilde{\theta} - \frac{3}{\tilde{w}} + \frac{\tilde{C}}{2}(\partial_X\tilde{w})^2.\end{aligned} \tag{5}$$

The dimensionless model Eqs. (1) and (5) depend on three dimensionless parameters: specific heat capacity, thermal conductivity, and capillarity coefficient:

$$\tilde{c}_v = \frac{c_v\theta_c}{p_c w_c}, \quad \tilde{k} = \frac{k\theta_c}{p_c w_c \zeta}, \quad \tilde{C} = \frac{C}{\zeta^2}, \tag{6}$$

with c_v the heat capacity at constant volume, k the coefficient of thermal conductivity, and C the capillarity coefficient. The system of Eqs. (1) and (5) is numerically solved using the Dedalus open-source code [32], which is based on a pseudospectral method. The model is solved using periodic boundary conditions and with homogeneous initial conditions $(w_0,\ p_0,\ \theta_0)$ in the disordered phase.

Pulses are stimulated by injecting a localized current (around $\tilde{X}_0$) with an amplitude A_{stim} for a brief time $(\tilde{t}_0)$. We focus on solitary pulses stimulated by locally increasing either the pressure or temperature for a brief duration. The dimensionless pressure stimulus is obtained by adding the following term into the density-pressure-temperature constitutive relation:

$$\tilde{p}_{\text{stim}}\Theta(\tilde{t}_0 - \tilde{t})\exp\left[-\frac{(\tilde{X}-\tilde{X}_0)^2}{2\lambda^2}\right]. \tag{7}$$

A localized temperature stimulus is obtained by adding the following term into the energy-temperature constitutive relation:

$$\tilde{c}_v\tilde{\theta}_{\text{stim}}\Theta(\tilde{t}_0 - \tilde{t})\exp\left[-\frac{(X-X_0)^2}{2\lambda^2}\right]. \tag{8}$$

Here, Θ is the Heaviside function and λ the width of the stimulus.

III. RESULTS

A. Information about the stimulus strength

Multiple properties of longitudinal pulses near a vdW phase transition were previously analyzed, including their characteristic shape and trajectory in phase space, and these details are given elsewhere [11]. Here, we examine the dependence of the peak density, pressure, and temperature of the pulse as the amplitude of the stimulus is increased. To stimulate a longitudinal pulse, we apply a local stress into

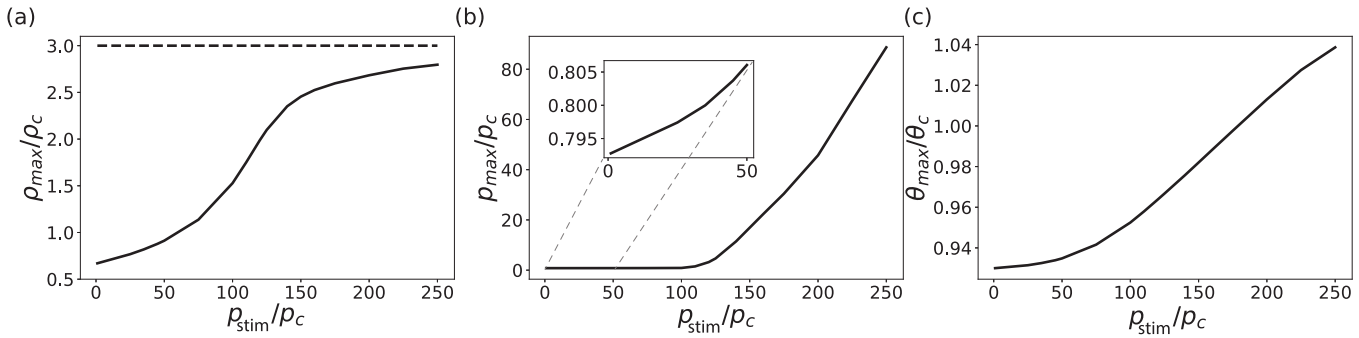

FIG. 1. Amplitude of (a) density, (b) pressure, and (c) temperature aspects of a solitary wave as a function of local mechanical stimulation strength, as calculated at a distance $\frac{x}{L} = 1.2$ from the stimulation point. Dashed line in (a) represents the maximum density allowed by the exclusion of volume. Parameter values are $(\tilde{c}_v, \tilde{k}, \tilde{C}) = (600, 100, 1)$, additional initial conditions are $(\tilde{w}_0,\ \tilde{v}_0, \tilde{\theta}_0) = (1.5, 0, 0.93)$, and stimulation parameters are $(X_0,\ \tilde{t}_0,\ \lambda) = (0, 0.1, 0.0625)$. Numerical calculation was conducted using 4096 grid points over an x domain $[-3\pi/2, 3\pi/2]$ and $d\tilde{t} = 3 \times 10^{-4}$.

the system by setting $A_{\text{stim}} = p_{\text{stim}}$ and adding Eq. (7) into the upper Eq. (5). Small-amplitude longitudinal waves cause a parallel incremental variation of the density, pressure, and temperature relative to their equilibrium values. By setting the equilibrium state close to the phase transition region in the low-density phase, the response of the three observables is significantly affected by the phase transition. At small amplitude of stimulation $\frac{p_{\text{stim}}}{p_c} < 50$, the response is almost linear, as shown in Fig. 1(a), the inset of Fig. 1(b), and Fig. 1(c). Increasing the amplitude of stimulation to larger values, $50 < \frac{p_{\text{stim}}}{p_c} < 120$ in Fig. 1, brings the system into the phase transition region. At this range of stimulation amplitude, a substantial increase in the amplitude of the density aspect is obtained because the system is softer in this region. At even stronger stimuli, $120 < \frac{p_{\text{stim}}}{p_c}$, the state reaches the high-density phase. Because of the exclusion of volume, the amplitude of the density aspect saturates at $\frac{\rho}{\rho_c} = 3$, while the pressure and temperature aspects do not, as shown in Figs. 1(a)–1(c), respectively.

Figure 1 demonstrates that the response of the density aspect to stimulus strength has a sigmoidal shape near the phase transition, as was previously shown [11]. In contrast, the response of the pressure and temperature is nonsaturating and resembles a smooth rectified linear unit (sReLU) function. Hence, longitudinal pulses near the phase transition carry both digitallike (sigmoidal) and analog (sReLU) information about the stimulus strength in different observables. Depending on the medium, additional observables that copropagate with the pulse can be considered. For example, in lipid membranes, variations in additional observables that propagate with the pulse include the charge density of the medium, transmembranal electric potential, and concentration of nearby ions [13]. Although not shown here explicitly, we find that the concentration of charged ions near the membrane, pH, and electric potential difference also demonstrate sigmoidal responses to stimulation, while the total energy shows an sReLU response.

B. Information about the stimulus type

We have previously shown that using different types of stimuli generate similar responses of the density aspect of longitudinal pulses that reversibly cross the phase transition. This was demonstrated by replacing the pressure stimulus with either temperature or energy stimuli [11]. Therefore, upon measuring the density aspect, it is challenging to deduce the source of stimulus, as shown in Fig. 2(a) for local pressure (solid black curve) and temperature stimuli (dotted-dashed yellow curve). In contrast, upon studying the pressure and temperature aspects, we recognize significantly different responses, as shown in Figs. 2(b) and 2(c), respectively. The trajectory of the signal in the $p - w$ plane of the vdW phase space is shown in Fig. 2(d). Evidently, the temperature stimulus generates a stronger response of the pressure and temperature observables than the pressure stimulus. Thus, the

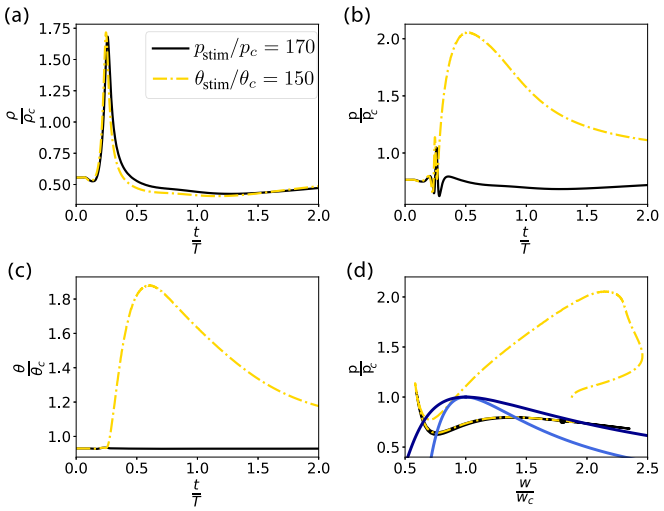

FIG. 2. Comparison of the (a) density, (b) pressure, and (c) temperature aspect responses at a distance $x/L = 1$ from the stimulation point, upon using either a pressure (solid black curve) or temperature (dotted-dashed yellow curve) stimulus. (d) Trajectory of the wave in the $p - w$ projection of the van der Waals (vdW) phase space. Initial state is marked with a black-filled circle. Dark-blue and blue curves represent the coexistence and spinodal curves, respectively. Parameter values: $\tilde{w}_0 = 1.8$. Other parameters are the same as in Fig. 1.

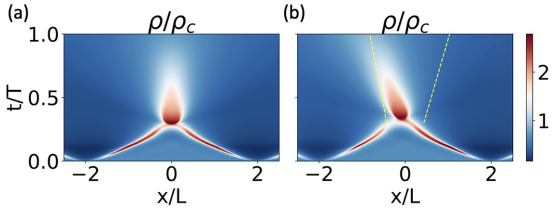

FIG. 3. (a) Numerical solution of density field as a function of space (x axis) and time (y axis) for two pulses in the nonlinear regime. Blue denotes the low-density phase and red the high-density phase. (b) Collision site is asymmetric when pulses have different amplitudes. Yellow dashed lines mark a region used to analyze the data presented in Fig. 4. Two stimuli were applied at $x/L = \pm 2$ with amplitudes of $\tilde{p}_{\text{amp}} = 190$ for the symmetric case and $\tilde{p}_{\text{amp}} = 190$ and 160 for the assymetric case. Other parameter values are the same as in Fig. 1.

transient change of both pressure and temperature carry information about the type of stimulus in addition to its amplitude.

C. Collision site as short-term memory

We now turn to examine the outcome of a head-on collision between two pulses. Collision sites do not exist in the linear regime, and two pulses penetrate one another. However, the transition from the linear to nonlinear response of the medium is accompanied by partial or complete annihilation, as shown in Fig. 3(a). This behavior is in accord with measurements in lipid monolayers [10]. The annihilation events—as calculated from the vdW fluid model—are associated with a long-lived nonequilibrium state whose spatial size can be ∼5 times the width of the pulse, and its duration is ∼5 times the duration of the pulse. The shape of the collision site, however, is sensitive to various properties of the colliding pulses, including the distance of the stimuli from one another and the amplitude of the two stimuli. The effect of the latter is exemplified in Fig. 3(b), showing how two pulses stimulated at different amplitudes generate an asymmetric collision site.

To illustrate how information about the two stimuli can be extracted from the collision site, we calculate the peak amplitude at the collision site and connect it to the amplitude of the two stimuli. The maximum values of the density, pressure, and temperature fields at the collision site are calculated in a region enclosed by the two dashed lines shown in Fig. 3(b). The results are plotted in Fig. 4 as a function of the amplitude of one stimulus, while the other is held fixed at $\frac{p_{\text{stim}}}{p_c} = 190$ (solid black curve), 160 (dotted-dashed dark red curve), and 140 (dashed blue curve), respectively. The peak of density and pressure shows variability depending on the amplitude of both stimuli [Figs. 4(a) and 4(b)], but the peak of temperature is sensitive mainly to the larger amplitude [Fig. 4(c)]. Hence, the temperature signal can pinpoint the peak of the larger amplitude. Subsequently, we can use the data from either the density or pressure fields to estimate the amplitude of the other stimulus.

IV. DISCUSSION

Many properties of longitudinal pulses that reversibly cross a vdW-like phase transition are like action potentials [7–11,13,14,33]. These similarities imply that it may be possible to harness longitudinal waves for *in materio* computing schemes using principles of biological or artificial neural network algorithms. The sigmoidal response is especially important because it provides a close analogy to the all-or-nothing nature of action potentials [34,35]. Herein, we showed that longitudinal pulses near a phase transition propagate in parallel a sigmoidal response of the density and electrical (in charged medium) aspects and an sReLU response of the pressure, temperature, and energy aspects. Interestingly, in recent years, it was demonstrated that, in artificial neural network models, a ReLU activation function shows better convergence performance than the sigmoidal activation function [36,37]. We find the observation that two functions so commonly used in artificial neural modeling emerge in hydrodynamics from the structure of the phase diagram is surprising and nonintuitive. Importantly, this result is general and requires no finetuning. These dependencies are a direct consequence of the soft nature of the coexistence of phases and the volume exclusion [11].

The parallel propagation of both digitallike and analog information about the stimulus means that longitudinal pulses carry more information than is typically considered in neuronal and artificial neural models (Fig. 1). An additional observation that stresses the importance of the multidimensionality of the signal is the insensitivity of the density aspect to different types of stimuli, as shown in Fig. 2(a). By reading the pressure or temperature aspects, we gain knowledge about the source of the stimulus not visible from the density or

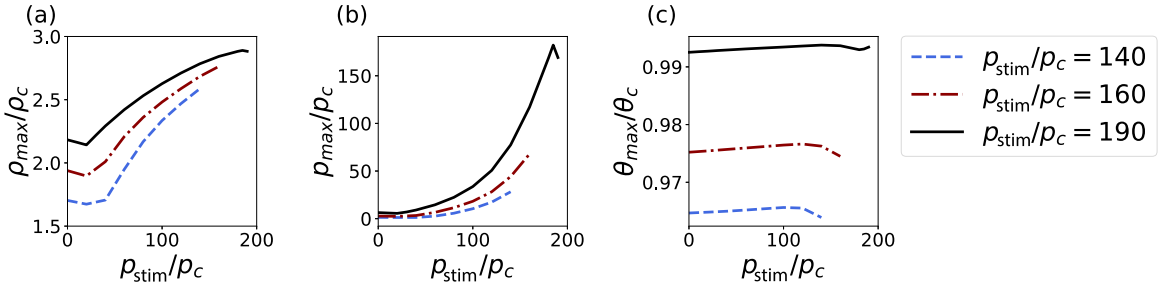

FIG. 4. The maximum value of the (a) density, (b) pressure, and (c) temperature aspects as calculated at the collision site [area enclosed by the two dashed lines in Fig. 3(c)] as a function of the stimulation amplitude. The second stimulus was held constant at $\frac{p_{\text{stim}}}{p_c} = 190$ (solid black curve), 160 (dotted-dashed dark red curve), and 140 (dashed blue curve), respectively. Parameter values are the same as in Fig. 1.

electrical aspects. Algorithms that could exploit the multidimensionality of the signal have not yet been considered.

From the experimental side, a practical system that can be used to stimulate these signals is a lipid membrane that includes a vdW-like phase transition at standard laboratory conditions of pressure and temperature. The emerging longitudinal pulses propagate at time and velocity scales that require only moderate sampling rate, respectively, $\sim 10^{-3}$ to 1 s and $\sim 10^{-1}$ to 10^{2} m/s [9,13]. In addition, the electrical aspect in charged lipid membranes becomes visible or hidden depending on the membrane charge density, which can be modified by changing the subphase acidity [13]. This provides a means to reveal or hide certain features of the digital aspect.

The longitudinal pulses discussed in this paper undergo dispersion and lose their velocity and structure over a distance of $\sim 3-10$ times the typical pulse size [11]. A way to overcome this issue of pulse dispersion would be via the subdivision of the computing substrate into interconnected compartments [38]. Such a network structure of lipid bilayers may be constructed using porous polymer sponges to produce millimeter-sized lipid interconnected compartments [39]. Subdivision of the medium into separate components further provides convenient degrees of freedom to tune the system into a desired response. This approach is referred to as physical learning and is usually achieved by choosing a learning rule that modifies these learning parameters [40]. Accordingly, the local mechanical characteristics of the lipid membrane may be treated as learning parameters since they directly modify the properties of the pulses. Since the mechanical parameters are closely linked to the geometrical structure of the membrane, these parameters may be tuned by locally exposing the membrane to external stimuli, such as pressure, temperature, or light [41–43].

In conclusion, nonlinear longitudinal pulses that reversibly cross a phase transition show a rich dynamical behavior that resembles neural activity and casts the information about the stimulus into a high-dimensional space. Consequently, these pulses could be useful to explore unconventional approaches for *in materio* computation.

ACKNOWLEDGMENT

The author thanks Shamit Shrivastava for introducing him to the field of *in materio* and reservoir computing and Menachem Stern for productive discussions.

[1] M. F. Hamilton and D. T. Blackstock, *Nonlinear Acoustics* (Academic Press, San Diego, 1998).

[2] *Rogue and Shock Waves in Nonlinear Dispersive Media*, edited by M. Onorato, S. Resitori, and F. Baronio (Springer, Cham, 2016).

[3] C. Kittel and H. Kroemer, *Thermal Physics*, 2nd ed. (Freeman, New York, 1997).

[4] T. Heimburg, *Thermal Biophysics of Membranes* (WILEY-VCH Verlag GmbH & Co. KGaA, Weinheim, 2008).

[5] M. S. Dimitriyev, Y.-W. Chang, P. M. Goldbart, and A. Fernández-Nieves, Swelling thermodynamics and phase transitions of polymer gels, Nano Futures **3**, 042001 (2019).

[6] S. G. Konarski, M. R. Haberman, and M. F. Hamilton, Acoustic response for nonlinear, coupled multiscale model containing subwavelength designed microstructure instabilities, Phys. Rev. E **101**, 022215 (2020).

[7] M. Mussel and M. F. Schneider, Sound pulses in lipid membranes and their potential function in biology, Prog. Biophys. Mol. Biol. **162**, 101 (2021).

[8] S. Shrivastava and M. F. Schneider, Evidence for 2D solitary sound waves in a lipid controlled interface and its implications for biological signaling, J. R. Soc. Interface **11**, 20140098 (2014).

[9] S. Shrivastava, K. H. Kang, and M. F. Schneider, Solitary shock waves and adiabatic phase transition in lipid interfaces and nerves, Phys. Rev. E **91**, 012715 (2015).

[10] S. Shrivastava, K. H. Kang, and M. F. Schneider, Collision and annihilation of nonlinear sound waves and action potentials in interfaces, J. R. Soc. Interface **15**, 20170803 (2018).

[11] M. Mussel and M. F. Schneider, Similarities between action potentials and acoustic pulses in a van Der Waals Fluid, Sci. Rep. **9**, 2467 (2019).

[12] M. Slemrod, Dynamic phase transitions in a van der Waals Fluid, J. Differ. Equ. **52**, 1 (1984).

[13] M. Mussel and M. F. Schneider, It sounds like an action potential: Unification of electrical, chemical and mechanical aspects of acoustic pulses in lipids, J. R. Soc. Interface **16**, 20180743 (2019).

[14] J. Griesbauer, S. Bössinger, A. Wixforth, and M. F. Schneider, Simultaneously propagating voltage and pressure pulses in lipid monolayers of pork brain and synthetic lipids, Phys. Rev. E **86**, 061909 (2012).

[15] D. Steppich, J. Griesbauer, T. Frommelt, W. Appelt, A. Wixforth, and M. F. Schneider, Thermomechanic-electrical coupling in phospholipid monolayers near the critical point, Phys. Rev. E **81**, 061123 (2010).

[16] H. Paugam-Moisy and S. M. Bohte, Computing with Spiking Neuron Networks, in *Handbook of Natural Computing*, edited by T. Bäck, J. N. Kok, and G. Rozenberg (Springer, Heidelberg, 2012), pp. 335–376.

[17] B. Yegnanarayana, *Artificial Neural Networks* (Prentice-Hall of India Private Limited, New Delhi, 2009).

[18] N. R. Shanbhag, S. Mitra, G. de Veciana, M. Orshansky, R. Marculescu, J. Roychowdhury, D. Jones, and J. M. Rabaey, The search for alternative computational paradigms, IEEE Des. Test Comput. **25**, 334 (2008).

[19] C. D. Schuman, T. E. Potok, R. M. Patton, J. D. Birdwell, M. E. Dean, G. S. Rose, and J. S. Plank, A survey of neuromorphic computing and neural networks in hardware, arXiv:1705.06963.

[20] F. Hadaeghi, X. He, and H. Jaeger, *Unconventional Information Processing Systems, Novel Hardware: A Tour d'Horizon* (Information Resource Center der Jacobs University, Bremen, 2017).

[21] C. Fernando and S. Sojakka, Pattern recognition in a bucket, in *Advances in Artificial Life*, edited by W. Banzhaf, J. Ziegler,

T. Christaller, P. Dittrich, and J. T. Kim (Springer, Berlin, 2003), pp. 588–597.

[22] G. Marcucci, D. Pierangeli, and C. Conti, Theory of Neuromorphic Computing by Waves: Machine Learning by Rogue Waves, Dispersive Shocks, and Solitons, Phys. Rev. Lett. **125**, 093901 (2020).

[23] S. Ma, T. M. Antonsen, S. M. Anlage, and E. Ott, Short-wavelength reverberant wave systems for physical realization of reservoir computing, Phys. Rev. Res. **4**, 023167 (2022).

[24] R. Cardona, E. Miranda, D. Peralta-Salas, and F. Presas, Constructing Turing complete Euler flows in dimension 3, Proc. Natl. Acad. Sci. USA **118**, e2026818118 (2021).

[25] *Collision-Based Computing*, edited by A. Adamatzky (Springer-Verlag, London, 2012).

[26] N. A. Silva, T. D. Ferreira, and A. Guerreiro, Reservoir computing with solitons, New J. Phys. **23**, 023013 (2021).

[27] E. M. Izhikevich and F. C. Hoppensteadt, Polychronous wavefront computations, Int. J. Bifurcation Chaos **19**, 1733 (2009).

[28] A. Pierro, K. Heiney, S. Shrivastava, G. Marcucci, and S. Nichele, Optimization of a hydrodynamic computational reservoir through evolution, arXiv:2304.10610.

[29] G. Marcucci, P. Caramazza, and S. Shrivastava, A new paradigm of reservoir computing exploiting hydrodynamics, Phys. Fluids **35**, 071703 (2023).

[30] B. U. Felderhof, Dynamics of the diffuse gas-liquid interface near the critical point, Physica **48**, 541 (1970).

[31] R. Courant and K. O. Friedrichs, *Supersonic Flow and Shock Waves* (Wiley-Interscience, New York, 1948), Vol. 21.

[32] K. J. Burns, G. M. Vasil, J. S. Oishi, D. Lecoanet, and B. P. Brown, Dedalus: A flexible framework for numerical simulations with spectral methods, Phys. Rev. Res. **2**, 023068 (2020).

[33] T. Heimburg and A. D. Jackson, On soliton propagation in biomembranes and nerves, Proc. Natl. Acad. Sci. USA **102**, 9790 (2005).

[34] J. R. Clay, Excitability of the squid giant axon revisited, J. Neurophysiol. **80**, 903 (1998).

[35] F. O. Schmitt and O. H. Schmitt, Partial excitation and variable conduction in the squid giant axon, J. Physiol. **98**, 26 (1940).

[36] A. Krizhevsky, I. Sutskever, and G. E. Hinton, ImageNet classification with deep convolutional neural networks, Commun. ACM **60**, 84 (2017).

[37] K. Gurney, *An Introduction to Neural Networks* (CRC Press, Boca Raton, 2018).

[38] J. Szymanski, J. N. Gorecka, Y. Igarashi, K. Gizynski, J. Gorecki, K.-P. Zauner, and M. De Planque, Droplets with information processing ability, Int. J. Unconv. Comput. **7**, 185 (2011).

[39] S.-I. M. Nomura, R. Shimizu, Richard J. Archer, G. Hayase, T. Toyota, R. Mayne, and A. Adamatzky, Spontaneous and driven growth of multicellular lipid compartments to millimeter size from porous polymer structures, ChemSystemsChem **4**, e202200006 (2022).

[40] M. Stern and A. Murugan, Learning without neurons in physical systems, Annu. Rev. Condens. Matter Phys. **14**, 417 (2023).

[41] F. M. Menger and M. I. Angelova, Giant vesicles: Imitating the cytological processes of cell membranes, Acc. Chem. Res. **31**, 789 (1998).

[42] S. Svetina, Vesicle budding and the origin of cellular life, ChemPhysChem **10**, 2769 (2009).

[43] C. Pernpeintner, J. A. Frank, P. Urban, C. R. Roeske, S. D. Pritzl, D. Trauner, and T. Lohmüller, Light-controlled membrane mechanics and shape transitions of photoswitchable lipid vesicles, Langmuir **33**, 4083 (2017).